Combustion, Explosion, and Shock Waves, Vol. 43, No. 3, pp. 258–275, 2007

Numerical Investigation of Turbulent Non-Premixed Combustion of a Wood Pyrolysis Gas

W. Pakdee[1] and Sh. Mahalingam[2]

UDC 534.222.2

Translated from *Fizika Goreniya i Vzryva*, Vol. 43, No. 3, pp. 15–34, May–June, 2007.
Original article submitted February 2, 2006; revision submitted September 25, 2006.

A fully compressible database of turbulent non-premixed flames of a wood pyrolysis gas is developed by means of direct numerical simulation (DNS). A reduced kinetic mechanism is used to model the combustion of a pyrolysis gas–air mixture. The instantaneous flame surface density evolution equation based on the concept of a displacement speed is examined. The normal component of the displacement speed is nearly constant with respect to curvature, while the curvature-related component tries to restore the flame front to a planar shape. The strain-rate term is mainly a source as the flame is mostly extended. The normal displacement is responsible for both positive and negative contributions to the flame area. The displacement/curvature term is primarily a sink, since it is dominated by its curvature component. Effects of strain and curvature are analyzed by considering their correlations with reaction rates. Reaction rates are enhanced with increased positive strain rates owing to an increase in the flame surface area and to a decrease in curvature. The analyzed results aid in the development of turbulent combustion models. Finally, a new model for a mean variance of the scalar dissipation rate, based on a scale similarity approach, is proposed and examined. A comparison with DNS results shows that the proposed model provides a significant improvement over existing models.

Key words: combustion, turbulent diffusion flame, direct numerical simulation, wood pyrolysis gas.

INTRODUCTION

Direct Numerical Simulation (DNS) of turbulent non-premixed flames is a useful tool in improving our understanding of complex interactions between combustion and turbulence. It also serves as an essential tool in the development and assessment of turbulent combustion models. Detailed investigations of fundamental physical processes may be conducted using DNS. Over the last decade, several researchers have carried out DNS to solve turbulent non-premixed flame problems [1–3]. The turbulence–chemistry interaction and turbulence effects on the flame structure have been investigated with the use of various chemistry models and flame configurations. Mahalingam et al. [4] used finite-rate two-step chemistry in their DNS study of transient effects on turbulent non-premixed flames. Bushe et al. [5] incorporated a two-step reduced mechanism for the combustion of a methane–air mixture with a nitrogen–oxygen mixture into a DNS code, with thermodynamic properties assumed to be constant. Another non-premixed DNS work was carried out to investigate autoignition of n-heptane–air combustion described by a single-step irreversible reaction [6]. Recently, a two-dimensional DNS was performed to study the burning modes (premixed versus non-premixed burning) in autoigniting mixtures of hydrogen in heated air [7].

In the case when chemistry is sufficiently fast, the chemical time scale is short compared to the convection and diffusion time scales. Consequently, combustion takes place within asymptotically thin elements embedded in the flame. These elements are called flamelets [8].

[1]Department of Mechanical Engineering, Thammasat University (Rangsit Campus), Pathumthani 12121, Thailand; wpakdee@engr.tu.ac.th.

[2]Department of Mechanical Engineering, University of California, Riverside, CA 92521, USA.

0010-5082/07/4303-0258 © 2007 Springer Science + Business Media, Inc.

In the flamelet regime, the burning rate can be estimated through the flame surface density (FSD) defined as the flame surface area per unit volume. The concept of the flame surface density was first introduced to describe non-premixed turbulent combustion by Marble and Broadwell [9]. An analysis of physical effects contributing to flame surface variation provides an understanding of how the flame surface is created, destroyed, distorted, and propagated due to a variety of mechanisms such as convection, curvature effects, and molecular diffusion. Different forms of the transport equation were introduced through geometrical considerations [9–11] or through a statistical approach [12, 13]. Based on a non-premixed combustion assumption, two equivalent exact transport equations for the isolevel surface density were derived [11]. One approach starts from a mixture fraction balance equation coupled with the definition of the flame surface density. In the other approach, the FSD transport equation is derived from the G-equation. The terms in the transport equations were extracted from DNS results and individually analyzed. Models for the unclosed terms were proposed. Van Kalmthout et al. [11] performed DNS of a constant-density mixing layer, assuming infinitely fast chemistry described by a single-step reaction with representative fuel and oxidizer. Van Kalmthout and Veynante [14] extended the work to account for heat-release effects with variable-density flows. An ideal gas was assumed with a constant specific heat ratio.

In our present work, we conduct DNS of turbulent non-premixed flames of a wood pyrolysis gas, which is a primary source of fuel to largely gaseous flames in an intense wildfire. In some situations of an intense fire, local meteorological conditions are substantially modified and could lead to a "blow up" [15]. For these intense conditions, the details of gas-phase combustion through which a large amount of energy is released need to be included in developing a physically sound fire model.

In the present work, the resulting database is introduced with descriptions of its fundamental features and statistics. The work has three primary objectives. The first objective is to examine individual terms contributing to the flame surface density evolution equation. As discussed earlier, a similar analysis was carried out for the flow configuration of a turbulent mixing layer modeled with a simple one-step reaction [11, 14]. Unlike their studies wherein the fuel is a pure gas, in our simulation the fuel is a pyrolysis gas comprised of a mixture of gases with more realistic chemical kinetics. The flame displacement speed and the role of curvature on FSD dynamics are physically interpreted and investigated. The relative importance of the curvature and strain rate is a subject of discussion, but little data are available for non-premixed flames. The past work related to this subject is mostly devoted to premixed flame investigations [10, 16–19]. This constitutes the second objective to present some preliminary findings with regard to the effects of the curvature and strain rate on the structure of the turbulent flame. Our third objective is motivated by the desire to develop a model for the mean variance of the scalar dissipation rate used for the flamelet model. A new approach based on the concept of scale similarity is introduced.

1. NUMERICAL PROCEDURE AND FLAME PARAMETERS

In the present study, we use a two-dimensional DNS of turbulent non-premixed flames of a wood pyrolysis mixture gas, which is a gaseous fuel mixture released from high-temperature pyrolysis of the ground fuel. This fuel is a complex mixture, including four main gases (CO, H_2, CH_4, and CO_2) [20]. The combustion of pyrolysis gas mixtures occurs through several hundred elementary reactions. Although a detailed reaction mechanism with an accurate description of the complex chemistry is possible, the computational cost is high. Therefore, a recently derived reduced four-step chemical kinetic scheme for modeling combustion of the wood pyrolysis gas is employed [21].

Numerical simulations of turbulent reacting flows involving such a complex chemistry remain very challenging owing to severe stiffness and nonlinearity of the governing equations including a large number of reactive species and a wide range of length and time scales. In the present work, a two-dimensional computational geometry is chosen, which makes feasible the inclusion of a more realistic chemistry. Although two-dimensional turbulence precludes physical effects like vortex stretching, previous studies have shown that the probability of finding locally three-dimensional spheroidal flames associated with the vortex stretching mechanism is much lower than the probability of finding two-dimensional cylindrical flame sheets [22]. Two-dimensional turbulence provided detailed statistical correlations similar to those of the three-dimensional case [14]. Domingo and Vervisch [23] carried out two- and three-dimensional turbulent combustion calculations. They investigated the role of triple flames and partially premixed combustion in the ignition processes of a non-premixed turbulent mixture. They found that two-dimensional calculations provided results similar to those of the three-dimensional case. Additionally, past research has shown that the difference between two- and three-dimensional effects on the dynamics and statis-

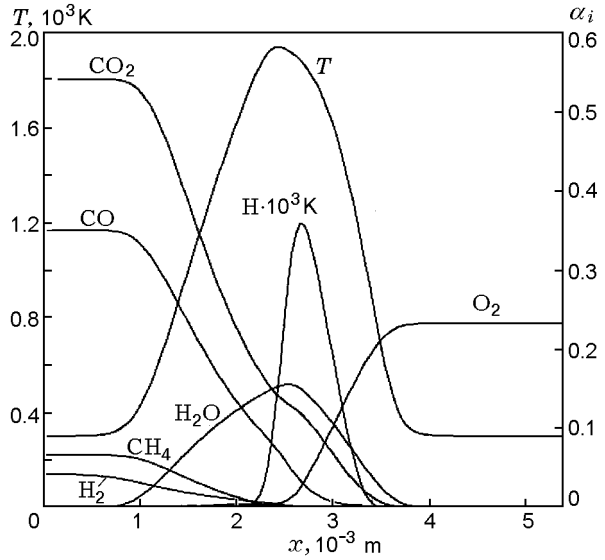

Fig. 1. Initial profiles of mass fractions (α_i) and temperature of opposed-flow diffusion flames for the wood pyrolysis gas.

tics of the flame surface are not significant [16, 24]. Thus, two-dimensional simulations can capture most of the turbulence-chemistry interactions. In recent years, many two-dimensional simulations have provided valuable results in turbulent reactive flows involving combustion [14, 17, 25].

The governing equations solved include mass, momentum, energy, and species conservation equations, which describe pyrolysis gas combustion [26]. A two-dimensional 1.0×1.0 cm domain with a uniform finite-difference grid resolution of 256×256, sufficient to resolve the smallest reaction zones, is utilized. An initially strained, one-dimensional laminar diffusion flame between the pyrolysis gas mixture and air is used, computed using an OPPDIF code [27]. The strain is removed as the flame becomes unstrained for the reaction-zone initialization. Initial profiles of reactant mass fractions and temperature are given in Fig. 1. A homogeneous turbulence field is "initialized" in the computational domain after the initial disturbance acoustic waves exit the domain. A fluctuating velocity field is generated. The Fourier transform of velocities is calculated in accordance with the turbulent kinetic energy Passot–Pouquet spectrum [28]. After that, a fast Fourier transform is used to reconstruct the velocities in the physical space. The initial turbulence Reynolds number based on the integral length scale is 118.

A compressible DNS code originally developed for combustion of perfect gases with constant specific heats [29] was modified to accurately treat mixture gases having variable thermodynamic properties with complex chemistry. Simple Fickian diffusion with the Lewis number approximation recommended by Smooke and Giovangigli [30] is employed as a transport model for individual species. Spatial derivatives are discretized using a sixth-order accurate compact finite-different scheme [31]. Such a scheme accurately model the behavior of the acoustic wave and ensures a reasonable spectral resolution for both amplitude and phase of the solution. Simulations at the boundary and in the nodes adjacent to the boundary have the third and fourth order of accuracy, respectively. A third-order Runge–Kutta scheme is used to integrate the equations in time. A modified Navier–Stokes characteristic boundary conditions (NSCBC) method described in detail in [26] is used to handle the boundary conditions. Nonreflecting boundary conditions are prescribed in the y direction. The x-direction boundary conditions are periodic.

A substantial computation in this study was conducted using parallel computers. The parallel algorithm was based on the method developed for the DNS of turbulent stratified shear flows [32]. The communication required among the computers is achieved by using the message passing interface (MPI) standard [33].

2. CHEMICAL KINETICS

Chemical reactions are modeled using a 4-step reduced mechanism recently developed in [21]. The model involves the reacting species CO, H_2, and CH_4, the combustion products H_2O and CO_2, and the radical H as an intermediate species. Other species (CH_3, CH_2O, HCO, O, OH, and HO_2) are assumed to be in a steady state. It was found that the partial equilibrium approximation introduced an error. This is due in part to the fact that CO and H_2 are part of the fuel in the oxidization process of the pyrolysis gas, unlike in hydrocarbon–air flames of pure gases where they are treated as intermediate species. The reduced reaction mechanism involves the reactions

$$\begin{aligned} &CH_4 + 2H + H_2O = CO + 4H_2, \\ &CO + H_2O = CO_2 + H_2, \\ &H + H + M = H_2 + M, \\ &O_2 + 3H_2 = 2H + 2H_2O. \end{aligned} \tag{1}$$

The reduced mechanism was validated using three test environments, which included a perfectly stirred reactor, a premixed flame, and an opposed diffusion flame [21]. Calculations performed with full, skeletal, and reduced chemistry over a wide range of pyrolysis fuel gas compositions, equivalence ratios, and strain rates,

are compared. By comparing the temperature distributions, species profiles, premixed flame speeds, and diffusion flame extinction conditions, it was found that the reduced mechanism generally provides a good description of the oxidation process of the pyrolysis gas [21]. The mass fractions of the pyrolysis fuel gas chosen in the present paper were $Y_{CO} = 0.35$, $Y_{H_2} = 0.042$, $Y_{CH_4} = 0.066$, and $Y_{CO_2} = 0.542$, representative of aspen wood [34].

3. TRANSPORT EQUATION FOR FLAME SURFACE DENSITY

Under the flamelet assumption, the diffusion flame is located near the stoichiometric isolevel $Z(\boldsymbol{x}, t) = Z_{st}$, where $\boldsymbol{x}$ is the spatial coordinate vector, t is the time, and Z is the mixture fraction defined for the pyrolysis gas mixture [21] as

$$Z = \frac{\dfrac{Y_C - Y_{C,ox}}{v_C W_C} + \dfrac{Y_H - Y_{H,ox}}{v_H W_H} + 2\dfrac{Y_{N,ox} - Y_N}{v_N W_N}}{\dfrac{Y_{C,f} - Y_{C,ox}}{v_C W_C} + \dfrac{Y_{H,f} - Y_{H,ox}}{v_H W_H} + 2\dfrac{Y_{N,ox} - Y_{N,f}}{v_N W_N}}, \quad (2)$$

where W is the molecular weight; the subscripts C, H, and N denote carbon, hydrogen, and nitrogen atoms, and the subscripts f and ox represent the initially unmixed fuel and oxidizer states, respectively. The coefficients v_C, v_H, and v_N are computed according to a simplified global reaction. With this definition of the mixture fraction, the peak temperature is very close to stoichiometric over a range of pyrolysis gas compositions. For the chosen pyrolysis gas composition burning with air, $Z_{st} = 0.226$. Since the flame front in non-premixed flames corresponds to a particular isolevel of the passive scalar, an exact expression for the FSD (Σ) can be obtained through the product of the magnitude of the scalar gradient and the "fine grained" probability density function (PDF) [14]:

$$\Sigma = |\nabla Z| \delta(Z - Z_{st}) \quad (3)$$

(δ is the Dirac delta function). The flame surface density balance equation was first developed in [9] to analyze turbulent diffusion flames. This derivation is based exclusively on phenomenological considerations.

An alternative formulation of the transport equation for Σ was derived in [14], based on the mixture fraction balance equation in the form of the G-equation

$$\frac{\partial Z}{\partial t} + \boldsymbol{u} \cdot \nabla Z = w |\nabla Z|, \quad (4)$$

where $\boldsymbol{u}$ is the velocity vector and w is the displacement speed.

The displacement speed w measures the isoscalar propagation speed relative to the flow field. An isosurface of the mixture fraction Z is considered. If this iso-Z-surface propagates in the normal direction in the flow field $\boldsymbol{u}$, similar to the premixed combustion case [10], the absolute propagation speed $\boldsymbol{v}$ of the iso-Z-surface is

$$\boldsymbol{v} = \boldsymbol{u} + w\boldsymbol{n}, \quad (5)$$

where the unit normal vector $\boldsymbol{n}$ of the iso-Z-surface is defined as pointing toward the oxidizer side:

$$\boldsymbol{n} = -\frac{\nabla Z}{|\nabla Z|}. \quad (6)$$

The displacement speed w is defined as

$$w = \frac{1}{\rho |\nabla Z|} \nabla \cdot (\rho \mathcal{D} \nabla Z)$$

$$= \underbrace{-\frac{1}{\rho |\nabla Z|} \frac{\partial}{\partial n} (\rho \mathcal{D} |\nabla Z|)}_{w_n} \underbrace{-\mathcal{D} \nabla \cdot \boldsymbol{n}}_{w_c}, \quad (7)$$

where $\dfrac{\partial}{\partial n}$ is the derivative along the flame normal vector $\boldsymbol{n}$ and $\mathcal{D}$ is the diffusion coefficient. The curvature $\mathcal{K} = \nabla \cdot \boldsymbol{n}$ is defined positive if the flame is convex toward the oxidizer. The first contribution w_n represents the displacement speed due to diffusive processes normal to the flame front at the stoichiometric mixture fraction. The second contribution w_c is related to the curvature of the iso-Z-surface. The transport equation for the instantaneous FSD is

$$\underbrace{\frac{\partial \Sigma}{\partial t}}_{\text{I}} + \underbrace{\nabla \cdot (\boldsymbol{u}\Sigma)}_{\text{II}} = \underbrace{(\nabla \cdot \boldsymbol{u} - \boldsymbol{n}\boldsymbol{n} : \nabla \boldsymbol{u})\, \Sigma}_{\text{III}}$$

$$\underbrace{- \nabla \cdot (w\boldsymbol{n}\Sigma)}_{\text{IV}} + \underbrace{(w \nabla \cdot \boldsymbol{n})\, \Sigma}_{\text{V}}. \quad (8)$$

The terms on the left-hand side correspond to the unsteady effect (I) and convection by the mean flow (II). The terms on the right-hand side correspond to the tangential strain rate acting on the surface (III), normal displacement of the flame front w (IV), and displacement/curvature effects (V). From the definition of the displacement speed w, the curvature term may be split into two contributions as [14]

$$w \nabla \cdot \boldsymbol{n} = w_n \nabla \cdot \boldsymbol{n} - \mathcal{D} (\nabla \cdot \boldsymbol{n})^2, \quad (9)$$

where the first contribution denotes effects due to the flame normal displacement. The second contribution represents flame surface destruction caused by the action of molecular diffusion in the wrinkled areas of the flame front. The terms appearing in Eq. (8) are examined in detail under results and discussion.

This formulation of the flame surface density is similar to the transport equation derived for premixed combustion [10, 35], where the balance equation for premixed combustion was derived. The transport equation was developed from the rate change of the flame front:

$$\frac{\partial \Sigma}{\partial t} + \nabla \cdot (\boldsymbol{u}\Sigma) = (\nabla \cdot \boldsymbol{u} - \boldsymbol{nn} : \nabla \boldsymbol{u})\,\Sigma - \boldsymbol{n} \cdot \nabla (w\Sigma). \quad (10)$$

The last term in this equation can be expressed as

$$\boldsymbol{n} \cdot \nabla (w\Sigma) = \nabla \cdot (\boldsymbol{n} w\Sigma) - w\Sigma \nabla \cdot \boldsymbol{n}. \quad (11)$$

The only difference between the transport equations (8) and (10) is in the definition of the displacement speed w. Unlike premixed flames where the displacement speed w can be estimated from the laminar flame speed S_l due to diffusion/reaction balance, in non-premixed combustion, the displacement speed w is governed by diffusive processes only.

4. MODEL FOR MEAN VARIANCE OF THE SCALAR DISSIPATION RATE WITH THE SCALE SIMILARITY APPROACH

A scale similarity model was proposed and successfully utilized for the subgrid-scale variance of the mixture fraction [36–38] used for large eddy simulations. The model is based on the idea that the largest unresolved scales have a structure similar to the smallest resolved structures. The goal in this section is to demonstrate that the scale similarity approach may be extended to estimate the variance of the scalar dissipation rate required in the flamelet model [8]. The scalar dissipation rate χ represents the rate of molecular mixing defined as

$$\chi \equiv 2\mathcal{D} \frac{\partial Z}{\partial x_j} \frac{\partial Z}{\partial x_j}. \quad (12)$$

In flamelet modeling, a turbulent diffusion flame is viewed as a statistical ensemble of thin laminar flames called flamelets [39]. The flamelet model assumes that, for turbulent flames, the local balance between the diffusion and the reaction is similar to one in a laminar counter flow diffusion flame [3]. The mean mass fractions and reaction rates are

$$\bar{Y}_i = \int_0^\infty \int_0^1 Y_i(Z,\chi) P(Z,\chi;x,t) dZ d\chi, \quad (13)$$

$$\bar{\dot{\omega}}_i = \int_0^\infty \int_0^1 Y_i(Z,\chi) P(Z,\chi;x,t) dZ d\chi, \quad (14)$$

where $Y_i(Z,\chi)$ describes the local flame structure and $P(Z,\chi;x,t)$ is the joint probability density function, PDF of Z, and its dissipation rate χ. The joint PDF accounts for the statistics of fuel–air mixing. A library of $Y_i(Z,\chi)$ is constructed by solving a laminar diffusion flame. The joint PDF $P(Z,\chi;x,t)$ may be modeled under the assumption that Z and χ are statistically independent. Therefore, $P(Z,\chi;x,t)$ can be written as

$$P(Z,\chi;x,t) = P(Z;x,t)P(\chi;x,t). \quad (15)$$

It is well known that the probability density function has been applied to develop subgrid scale closures in turbulent combustion modeling [40–43]. PDFs on the right-hand side of Eq. (15) can be modeled. A beta-function is assumed for $P(Z;x,t)$ [44]. Discussions on modeling $P(\chi;x,t)$ are presented below.

Approach and Formulation

Peters [45] approximated $P(\chi;x,t)$ using a well-known log-normal distribution to determine the probability of burning flamelets:

$$P(\chi;x,t) = \frac{\exp\Big(-\frac{1}{2\sigma^2(x,t)}\left(\ln\chi - \gamma(x,t)\right)^2\Big)}{\sqrt{2\pi}\chi\sigma(x,t)}. \quad (16)$$

Here the parameters σ and χ are related to the first and second moments of the scalar dissipation rate by

$$\bar{\chi} = \exp\left(\gamma + \frac{\sigma^2}{2}\right), \quad (17)$$

$$\overline{\chi'^2} = \bar{\chi}^2(\exp(\sigma^2) - 1). \quad (18)$$

Models for the mean scalar dissipation rate $\bar{\chi}$ have been proposed [37, 46, 47]. It was found from the experiments that σ^2 should be close to unity [48, 49]. Once σ is known, the parameter γ can be computed. Consequently, the PDF $P(\chi;x,t)$ can be obtained from Eq. (16).

In this paper, we focus on the mean variance of the scalar dissipation rate $\overline{\chi'^2}$, which is defined as [36]

$$\overline{\chi'^2} = \overline{\chi^2} - \bar{\chi}^2. \quad (19)$$

A simpler alternative to modeling $\overline{\chi'^2}$ by using a scale similarity model is proposed. This approach was successfully applied in modeling the variance of a passive scalar mixture fraction [37, 50]. Recently, scale similarity of the scalar dissipation rate was assumed in developing dynamic structure models for large eddy simulation [51]. Thus, $\overline{\chi'^2}$ can be modeled as

$$\overline{\chi'^2} \cong c(\widehat{\bar{\chi}^2} - \widehat{\bar{\chi}}^2), \quad (20)$$

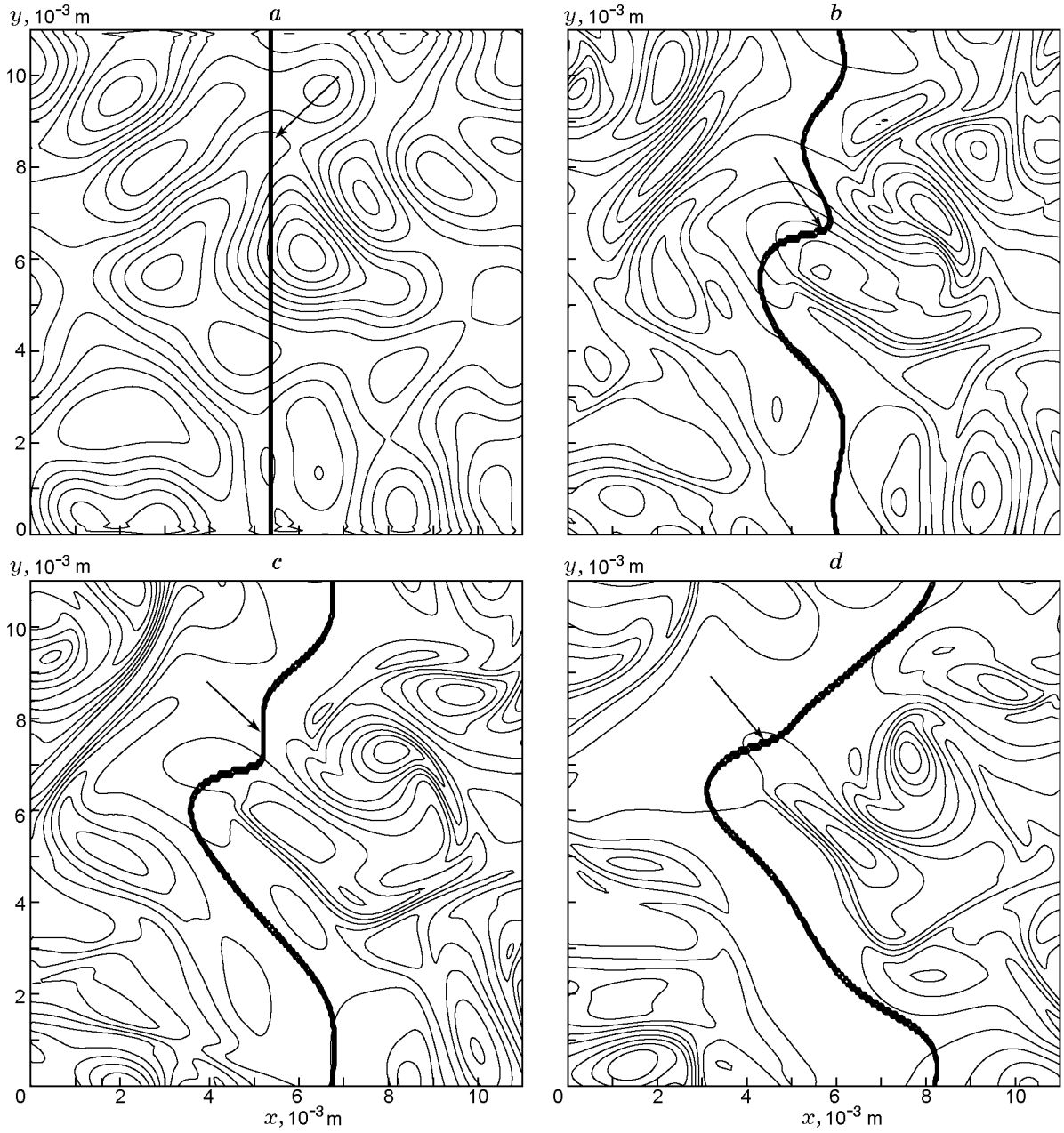

Fig. 2. Equispaced vorticity contours overlaid by equispaced flame surface density contours (indicated by arrows) with 10 levels: vorticity contours ranging from -2377.19 to 3146.54 sec^{-1} (a), from -9856.26 to 8158.42 sec^{-1} (b), from -9337.52 to 7007.6 sec^{-1} (c), and from -8816.56 to 6439.8 sec^{-1} (d).

where c is a scale similarity constant; the test filter with a size larger than the filter grid is marked by hat symbol. The filter operation used is defined in Sec. 5.3. The right-hand side term of Eq. (20) is contributed by eddies with sizes ranging from the filter gird scale to the test filter scale. The parameters γ and σ can be easily derived in terms of $\overline{\chi'^2}$ and $\bar{\chi}$:

$$\gamma = \ln \bar{\chi} - \left(\frac{\overline{\chi'^2}}{\bar{\chi}^2} + 1 \right) \Big/ 2, \tag{21}$$

$$\sigma = \sqrt{\ln \left(\frac{\overline{\chi'^2}}{\bar{\chi}^2} + 1 \right)}. \tag{22}$$

This model and the previous models are compared and assessed using DNS data. The results are given in Sec. 5.3.

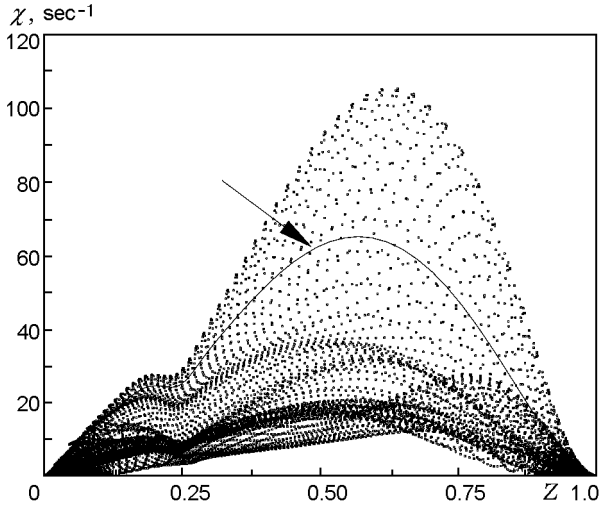

Fig. 3. Scatter plots of the scalar dissipation rate at $t = 0.75t_e$: the solid curve (indicated by the arrow) is the laminar prediction; data points are skipped every 3 points in the y direction.

5. RESULTS AND DISCUSSION

5.1. FSD Transport Equation

From phenomenological considerations, the FSD may also be defined as the flame surface area δA comprised in a volume [14]:

$$\delta A = \int_{\delta V} \Sigma dV. \tag{23}$$

This method is useful to estimate the FSD from DNS data. In a two-dimensional configuration, it involves calculation of the flame length within a mesh area $\Delta_x \Delta_y$.

The resulting computational fields were then extracted and investigated. Figure 2 displays the contours of instantaneous vorticity and DNS results for the flame surface density at different turbulence interaction times, based on the initial eddy turnover time $t_e = l_t/u_t$, where l_t is the initial integral length and u_t is the initial turbulent velocity. The initially planar laminar flame is stretched and distorted by the turbulence. However, vorticity near the flame zone is weakened both due to an increase in kinematic viscosity with temperature and volumetric expansion. As the turbulence distorts the flame, peak FSD values appear near the curved regions of the flame front. Aside from the FSD, the scalar dissipation rate χ is a useful measure of the behavior of non-premixed combustion. A scatter plot of χ versus the mixture fraction at the time $t = 0.75t_e$ is shown in Fig. 3. The solid curve indicated by the arrow represents the results for the laminar flame. Owing to turbulence, a considerable scatter of the scalar dissipation rate departing from the laminar flame prediction is observed. The peak values appear around the mixture fraction $Z = 0.6$. There exists a shoulder profile in both laminar and turbulent cases around the location of the stoichiometric mixture fraction $Z_{\rm st}$. This location corresponds to the flame region where energy is released. The high viscosity in this location levels off the gradients of the mixture fraction, thereby reducing the values of χ.

Figure 4 is a scatter plot of the instantaneous normal displacement speed w_n as a function of the mixture fraction Z at three different times during the interaction of turbulence with the flame. The laminar and turbulent cases have the same overall trend. The normal displacement speed w_n is induced by diffusion processes normal to the mixing zone, which thickens with time [14]. In the fuel region, the iso-Z-surfaces have negative values of w_n, as the surfaces displace toward the fuel side. In the oxidizer region, the displacement speeds w are mostly positive. This indicates that iso-Z-surfaces move toward the oxidizer side and displace away from the central region. In a small region near $Z_{\rm st}$, however, slightly negative values of w_n are observed. This result suggests that the fuel is locally deficient, causing the isosurfaces to propagate toward the fuel side. Note, in the neighborhood of $Z_{\rm st}$, the straining motion induced by the turbulence causes the iso-Z surfaces to displace toward one another. This is evident by the fact that the normal displacement speeds w_n are positive (negative) for $Z > Z_{\rm st}$ ($Z < Z_{\rm st}$).

As given in Eq. (9), the displacement speed w has two contributions. Figure 5 shows the variation of the displacement speed with curvature and its contributions along the stoichiometric line. As expected, the

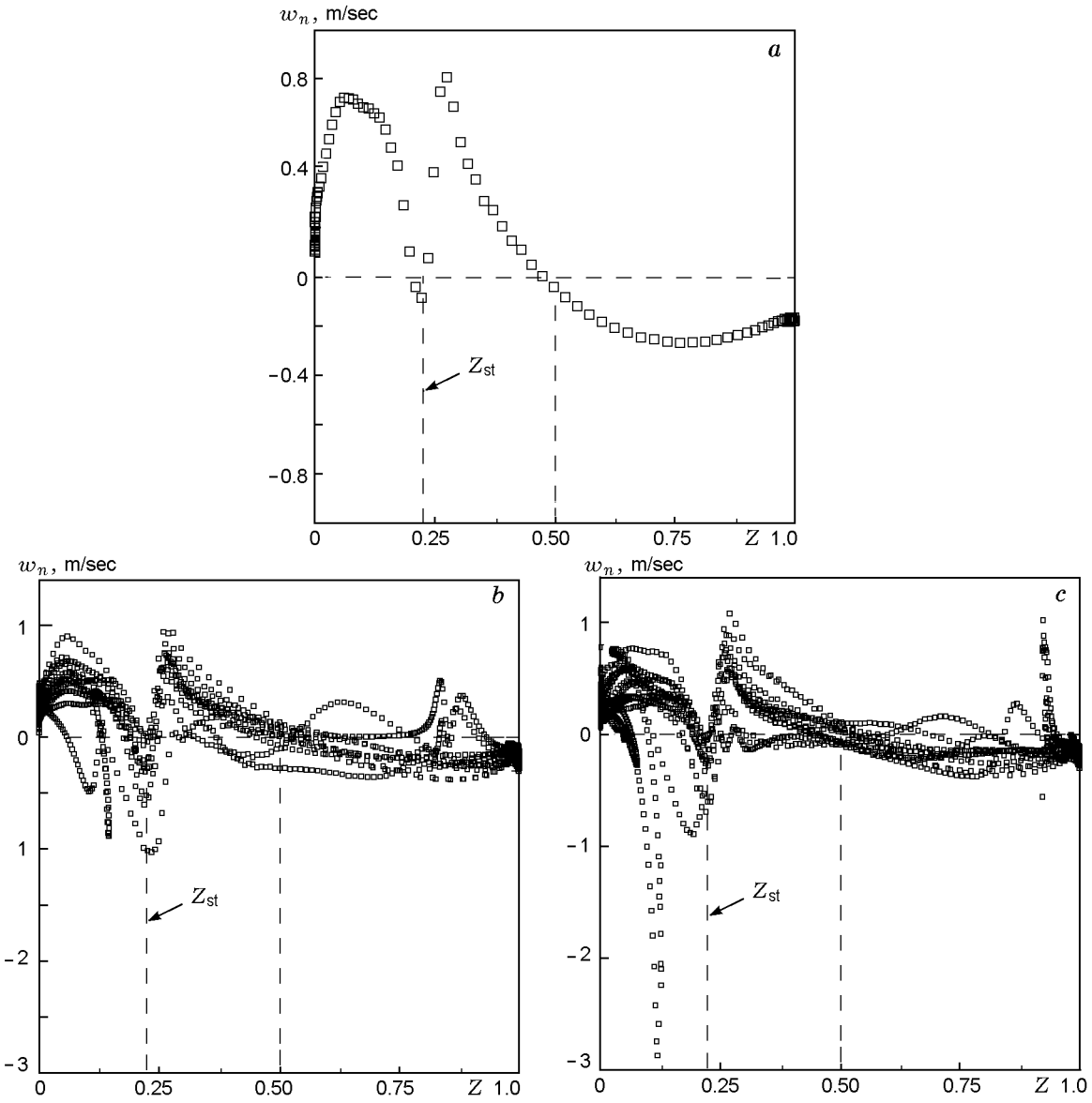

Fig. 4. Scatter plots of the normal displacement speed w_n as a function of the mixture fraction at $t = 0$ (a; laminar regime) and $t = 0.5t_e$ and $1.0t_e$ (b and c, respectively; turbulent regime); data points are skipped every 15 points along the y direction.

curvature-related displacement speed w_c, which is inversely proportional to curvature, is positive (negative) at negative (positive) curvature and vanishes at zero curvature. As a result, the flame surface is displaced toward the fuel (oxidizer) stream at positive (negative) curvature. In other words, it moves in the direction to pull back the flame surface to its planar shape. The normal displacement speed w_n appears to be weakly curvature dependent. It has mostly negative values with smaller magnitudes. This result is consistent with that observed in Fig. 4. By virtue of this fact, the curvature-related displacement speed w_c contributes more significantly to the total displacement speed w.

The instantaneous values of the terms in the FSD transport equation are illustrated in Fig. 6. It is evident that the strain rate term (III) primarily behaves as a source leading to an increase in the flame surface area by local straining. The normal displacement term (IV) is larger in magnitude. Its effect is basically a convection process leading to displacement of an iso-Z-surface. Its values are close to zero near $Z_{\rm st}$. This term behaves mainly as a sink on the oxidizer side. On the

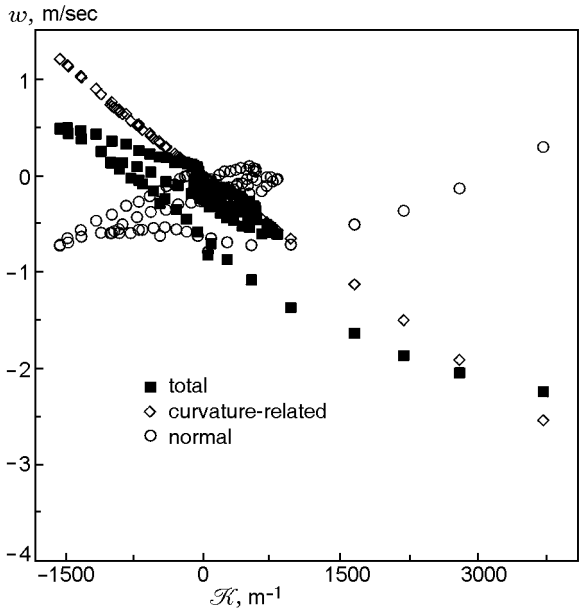

Fig. 5. Scatter plots of the displacement speed w as a function of curvature at $t = t_e$.

other hand, it behaves mainly as a source associated with significant positive values in the region toward the fuel. The curvature term (V) with its two contributions is illustrated in Fig. 7. The displacement component is responsible for both surface creation and destruction. The curvature component, however, acts as a pure sink term as it restores the flame surface back to its planar shape, thereby destroying the flame surface. This curvature component has a considerably larger order of magnitude than the displacement component. Therefore, the curvature term (V) is primarily a sink.

Plots of this dominant curvature contribution [see Eq. (9)] to the curvature/displacement term (V) at different times are given in Fig. 8. It is found as expected that this term is a sink. The magnitude of this term tends to increase with larger curvature magnitudes. It would contribute more significantly if the values of curvature are higher, as is expected at higher turbulence Reynolds numbers.

5.2. Turbulence Effects: Strain Rate and Curvature

To gain a better understanding of the evolution of various scalar variables characterizing turbulence, Favre averaging is performed at each x along the y axis. These Favre-averaged quantities as a function of x are depicted in Fig. 9 at the initial and later times corresponding to $t = 0.25t_e$, $0.5t_e$, $0.75t_e$, and t_e. The Favre averages of the x component velocity

$$\tilde{u}_x = \frac{\overline{\rho u}}{\bar{\rho}}, \tag{24}$$

where ρ is the fluid density, are shown in Fig. 9a. It can be seen that the dilatation effect by heat release in the flame zone induces the flame to move away from the central region. In Fig. 9b, the overall scalar dissipation rate reduces with time as turbulence decays. The Kolmogorov length scale [5]

$$\eta = \left(\frac{\tilde{\nu}^3}{\tilde{\varepsilon}}\right)^{1/4}, \tag{25}$$

where $\tilde{\nu}$ and $\tilde{\varepsilon}$ denote the Favre-averaged kinematic viscosity and the Favre-averaged kinetic energy dissipation rate, respectively, is depicted in Fig. 9c, and the Favre-averaged dissipation rate of turbulent kinetic energy given by the formula [52]

$$\tilde{\varepsilon} = \frac{\overline{\rho\nu\left(\frac{\partial u_i}{\partial x_j} + \frac{\partial u_j}{\partial x_i}\right)^2}}{\bar{\rho}} \tag{26}$$

is shown in Fig. 9d. The Kolmogorov lengths decrease in time in the central region of the domain (in the vicinity of the flame) because of high viscosity, while increasing away from the center due to decaying of turbulence. Similar overall trends are observed for the Favre-averaged energy dissipation rate. Considering the definition of η suggests that the kinematic viscosity is the dominant parameter over the energy dissipation rate.

To better understand the turbulent flame structure and the turbulence–flame interaction, instantaneous contours of the CH_4 reaction rate and the corresponding scalar dissipation rate are examined in Fig. 10. High values of the reaction rate appear where the flame is relatively flat. The reaction rate peaks are located near a region of a high scalar dissipation rate, where the mixing rate is high. Accordingly, the reaction rates are enhanced as the rate of supply of reactants increases. Peak values of χ appear closer to the fuel side. Its gradients are levelled off in the location of the flame, causing a shoulder profile exhibited in Fig. 3. Although the reaction zone experiences strong curvature and strain effects, the structure of the reactive zone itself does not appear to be modified by the turbulence. This is due to the high viscosity in the reactive zone, which weakens the turbulence intensity. This suggests that the flamelet concept is applicable in this case.

To gain additional insight into the turbulence–combustion interaction, correlations of the reaction rate with the strain rate and curvature are analyzed. The strain rate is associated with the rate of tangential strain acting on the flame surface [10, 14] and is given by

$$a_t = \nabla \cdot \boldsymbol{u} - \boldsymbol{nn} : \nabla \boldsymbol{u}. \tag{27}$$

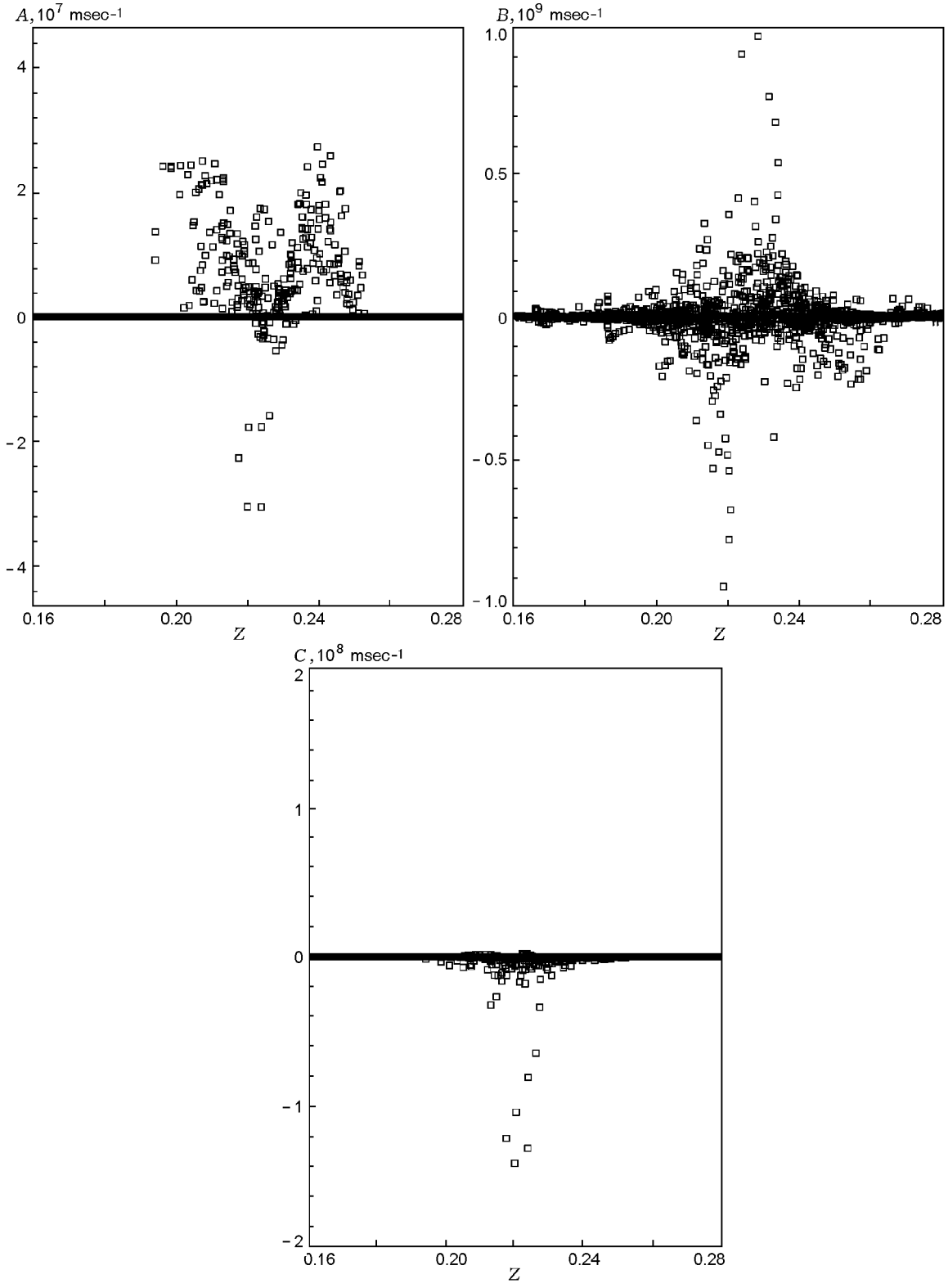

Fig. 6. Scatter plots of the instantaneous values of the terms in the flame surface density transport equation at $t = t_e$: A, B, and C are terms III, IV, and V of Eq. (8), respectively; the stoichiometric mixture fraction is $Z_{\rm st} = 0.226$.

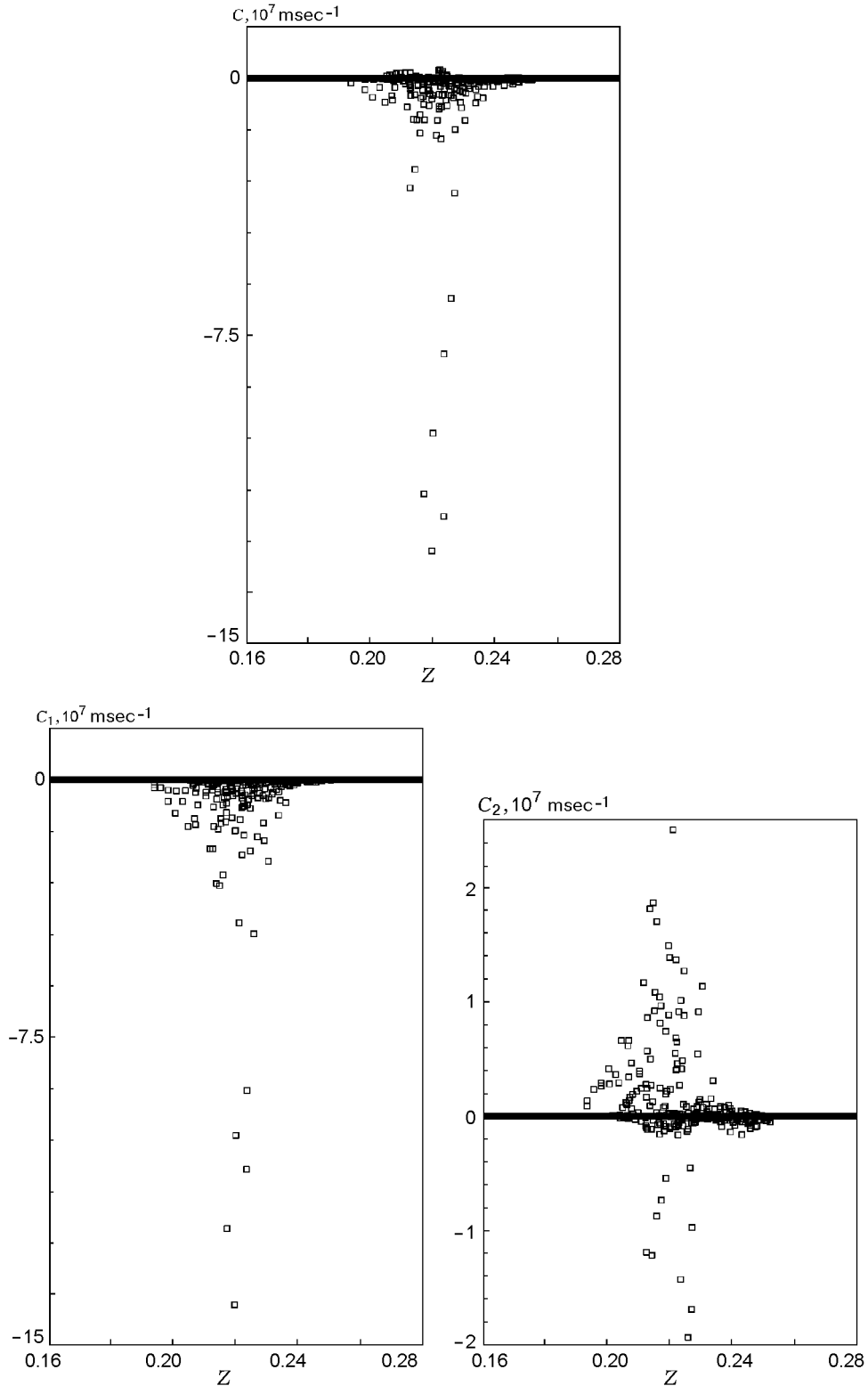

Fig. 7. Scatter plots of the instantaneous values of the displacement/curvature term C [term V of Eq. (8)] and its curvature component C_1 and displacement component C_2 [Eq. (9)] at $t = t_e$.

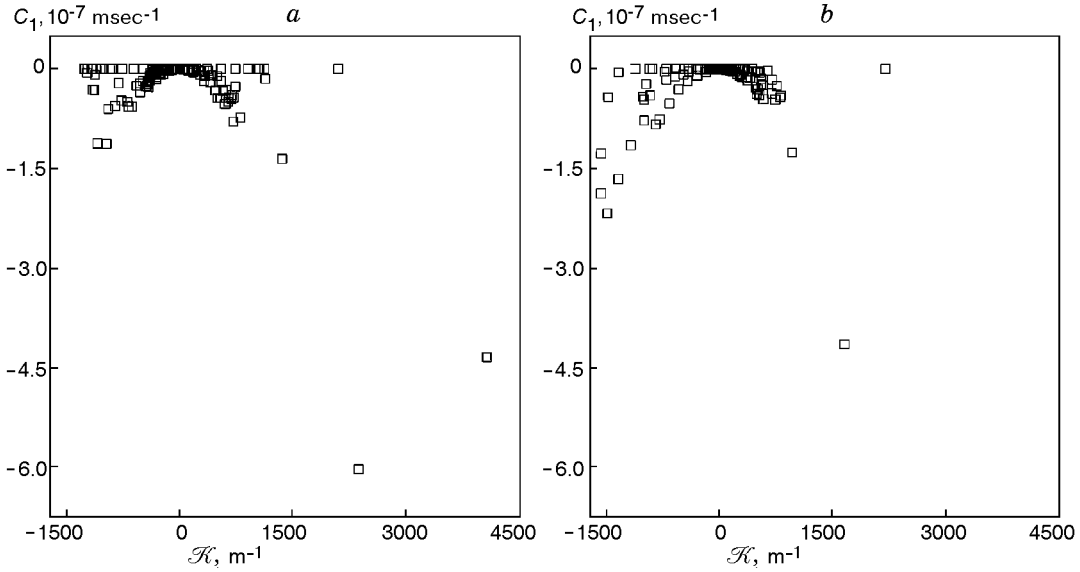

Fig. 8. Scatter plots of the instantaneous values of the curvature component term [Eq. (9)] as a function of curvature along the $Z_{\rm st}$ line at $t = 0.5t_e$ (a) and t_e (b).

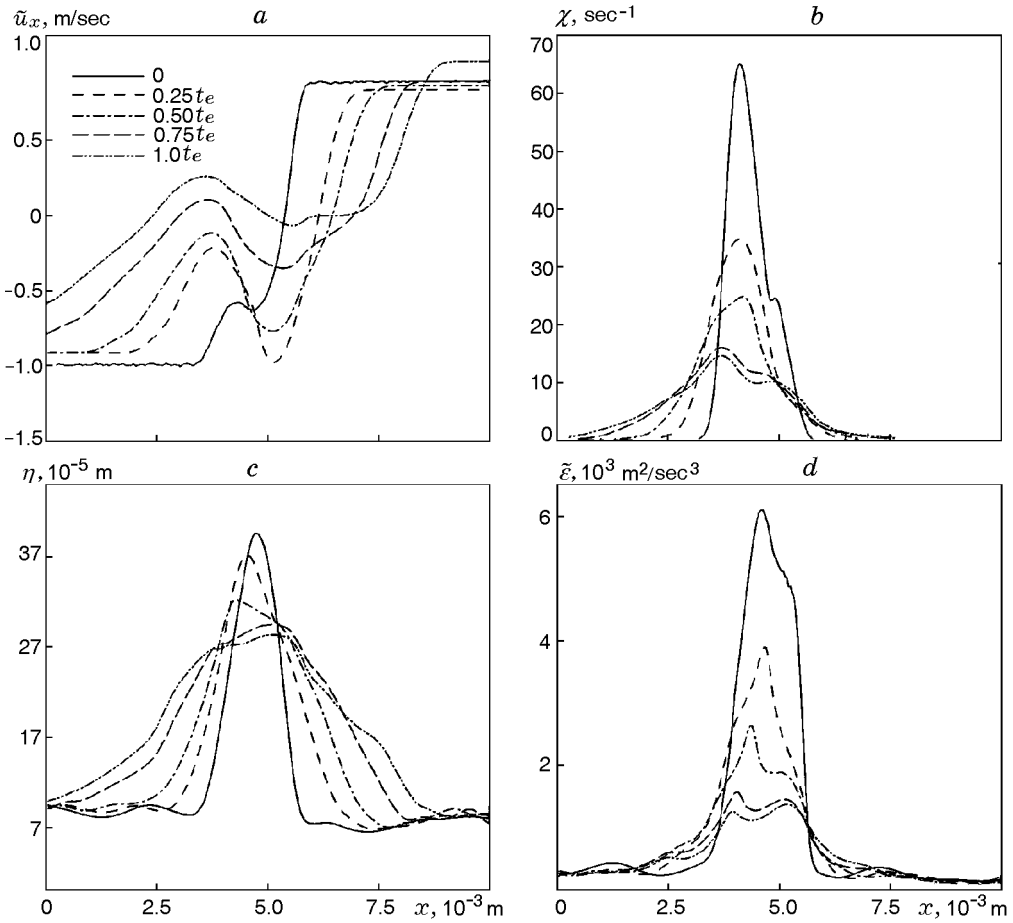

Fig. 9. Plots of the Favre-averaged quantities of the x-component velocity (a), scalar dissipation rate (b), Kolmogorov length (c), and energy dissipation rate (d) as a function of x at different times.

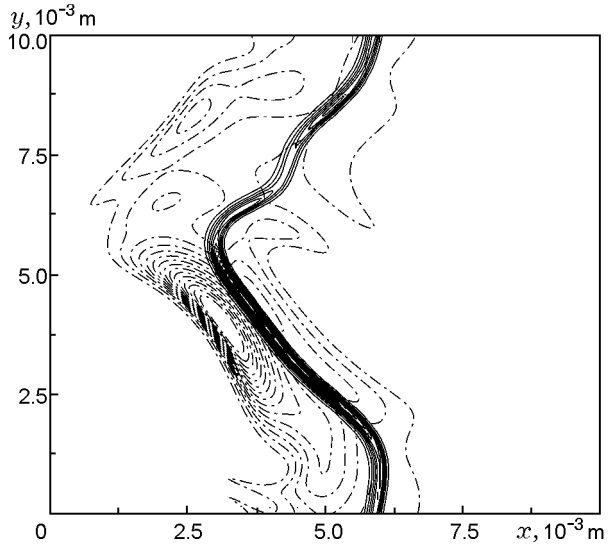

Fig. 10. Equispaced contours with 15 levels of the scalar dissipation rate (dot-and-dashed curve) overlaid by the reaction rate of CH_4 (solid curve) at $t = 0.75t_e$: the contours of the dissipation rate and the CH_4 reaction rate range from 6.2 to 92.7 sec^{-1} and from 1.9 to 28.3 kg/m^3, respectively.

Once again, the curvature $\mathcal{K}$ is defined positive if the flame is convex toward the oxidizer [14].

Figure 11 is a scatter plot of the CH_4 reaction rate and the strain rate at several times. It can be concluded from these statistics that the magnitudes of the CH_4 reaction rate are very close to zero in regions of negative stain rates and increase with increasing positive strain rates. This is caused by an increase in the flame surface area due to straining. As the time increases, most data points are clustered together at the value of the strain rate close to 1200 sec^1. A scatter plot of the CH_4 reaction rate with $\mathcal{K}$ is shown in Fig. 12. The reaction rate increases as the curvature decreases and reaches a maximum value near zero curvature with time. This is consistent with the region of the peak reaction rate observed in Fig. 10. The correlation of the strain rate with curvature at different times is illustrated in Fig. 13. It can be seen that positive strain rates increase and negative strain rates decrease with decreasing curvature $\mathcal{K}$. These results suggest that the strained flame tends to extend when the curvatures decrease. The peak strain rate appears at around zero curvature and may be associated with the maximum reaction rate observed in Figs. 11 and 12. Notice from Figs. 11–13 that the degree of scatter becomes smaller at later times due to weakened turbulence. The other marked statistical trend is that most of the data points correspond to positive strain rates, resulting in their statistical average being positive, while the averaged curvature is close to zero. This

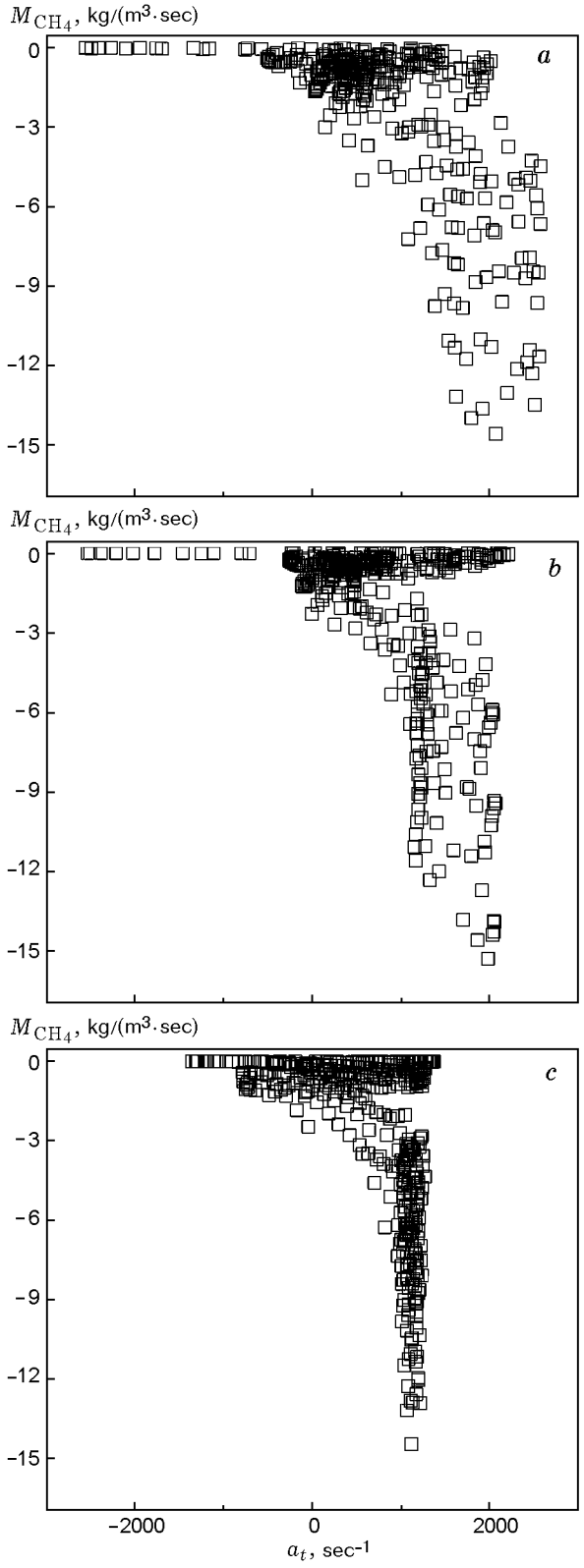

Fig. 11. Scatter plots of the CH_4 reaction rate as a function of the strain rate at $t = 0.2t_e$ (a), $0.5t_e$ (b), and t_e (c).

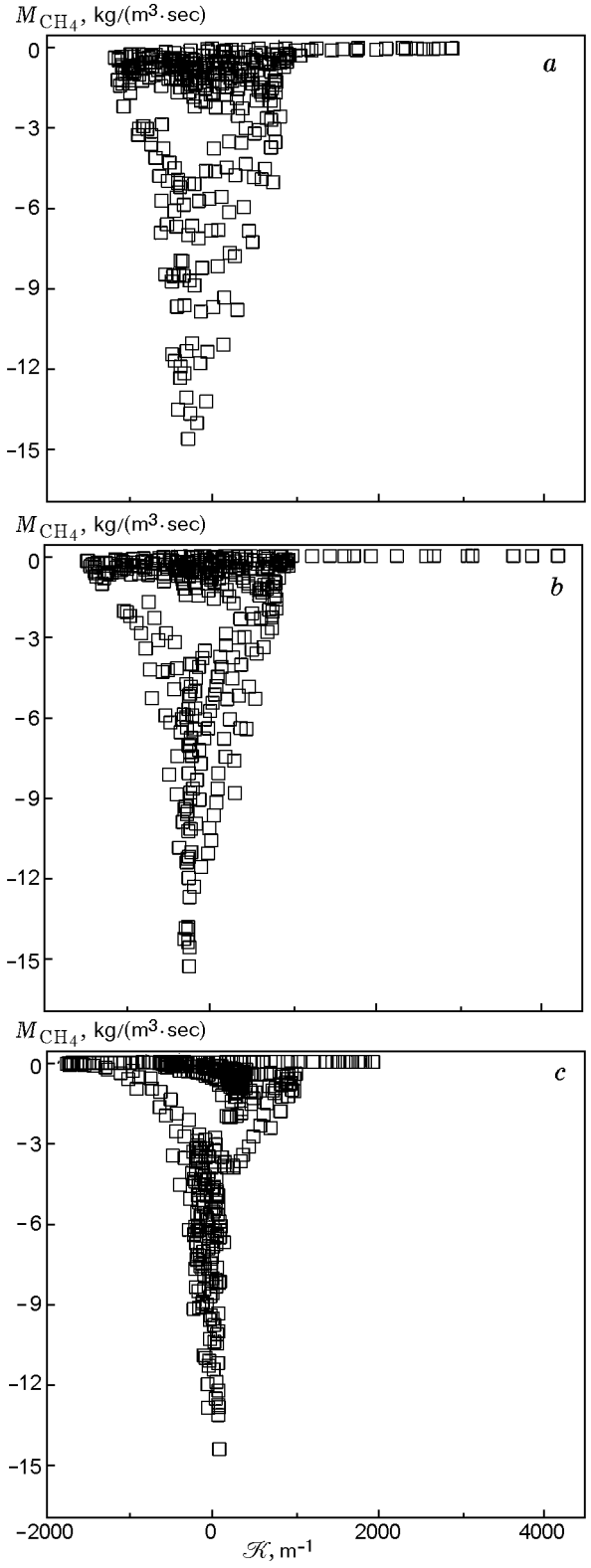

Fig. 12. Scatter plots of the CH_4 reaction rate as a function of curvature at $t = 0.2t_e$ (a), $0.5t_e$ (b), and t_e (c).

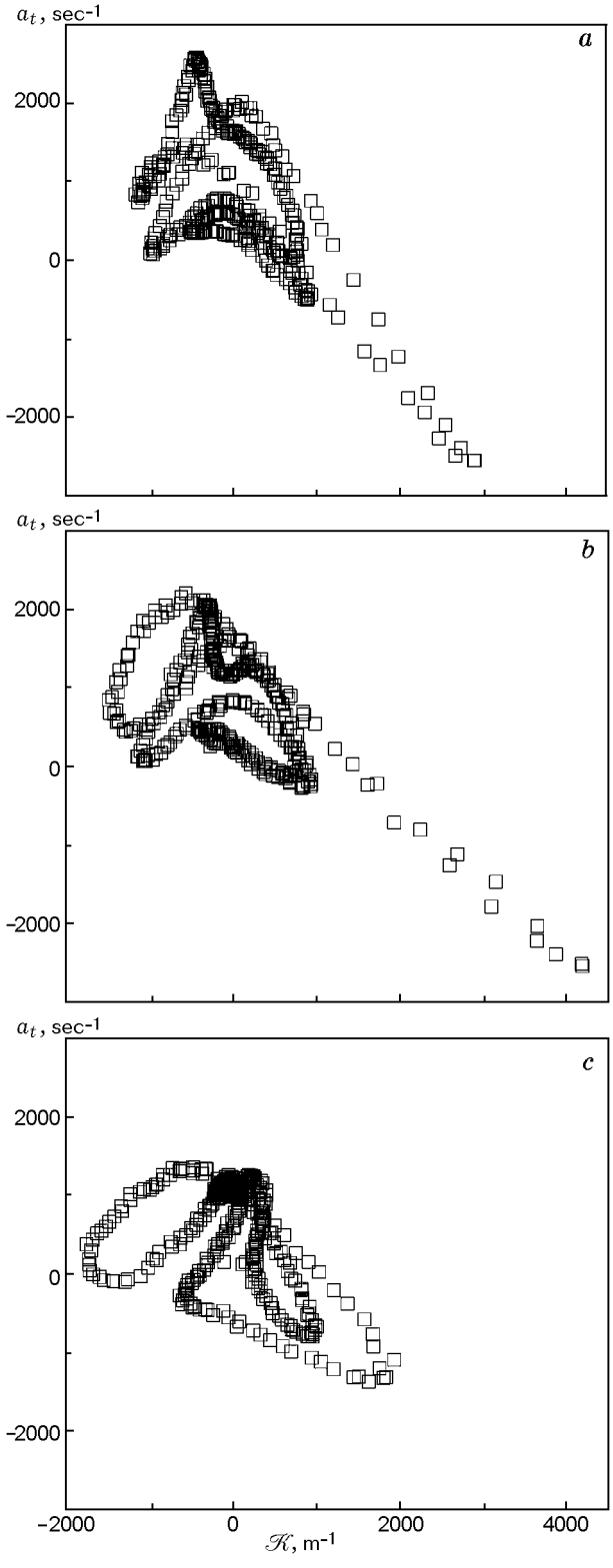

Fig. 13. Scatter plots of the strain rate as a function of curvature at $t = 0.2t_e$ (a), $0.5t_e$ (b), and t_e (c).

result is consistent with previous works observed in premixed flame combustion [17, 53].

5.3. Model for the Mean Variance of the Scalar Dissipation Rate

In this section, the capability of the scale similarity model in estimating the mean variance of the scalar dissipation rate, previously presented in Sec. 4, is investigated. The mean variance of the scalar dissipation rate modeled by the scale similarity assumption [Eq. (20)] and the previous model calculated by Eq. (18) are tested *a priori*. The DNS database with a larger domain of 2.0×2.0 cm, considered in [25], is employed. The DNS data with 512×512 resolution are filtered and used for the purpose of assessment. The filtered value $\overline{f}$ of the quantity f is

$$\overline{f}(\boldsymbol{x}, t) = \frac{1}{\Delta} \int_0^{\Delta} f(\boldsymbol{x}', t) d\boldsymbol{x}', \tag{28}$$

where Δ has a size of 32 cells of the DNS grid. In this investigation, the parameter σ equal to unity is used, as suggested in [48, 49]. Estimates of $\overline{\chi'^2}$ can be computed by both models. Figure 14 shows the equispaced isocontours of the mean variance of χ calculated by the previous model and the new scale similarity model; the values computed directly from DNS data are also plotted. To facilitate a direct comparison, the contours in all figures have the same 20 levels. It is clear from the comparison that the contour profiles predicted by the proposed model are much more similar to those calculated from DNS than those from the previous model predictions. To further examine the results, scatter plots comparing the modeled values of $\overline{\chi'^2}$ with actual DNS values are shown in Fig. 15 for the previous model and the new scale similarity model. Each figure shows a line of unity slope representing the exact model. It can be easily seen that the data points of $\overline{\chi'^2}$ computed by the scale similarity model match the actual DNS values reasonably well, while previous model predicts the values poorly, as their magnitudes are too large. To perform quantitative comparisons of the models, we calculated the variance (ε) of the modeled quantity x by the formula

$$\varepsilon = \left[\frac{\sum_{i=1}^{N} (x_{i\mathrm{mod}} - x_{i\mathrm{DNS}})^2}{\sum_{i=1}^{N} (x_{i\mathrm{DNS}})^2} \right]^{1/2},$$

where N is the number of data points and the subscript i refers to the data point. The values of ε calculated by the previous and proposed models are 21.04 and 0.39, respectively. Predictions of $\overline{\chi'^2}$ are greatly improved by using the scale similarity model.

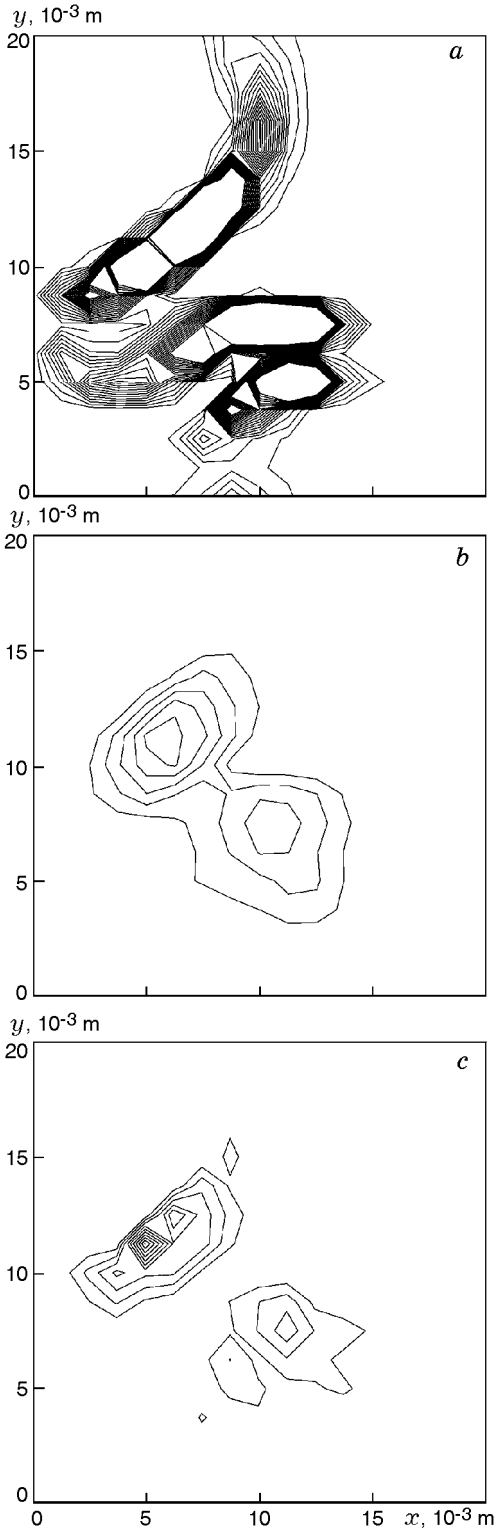

Fig. 14. Equispaced contours with 20 levels ranging within $\overline{\chi'^2} = 0$–7000 sec^{-1} obtained by the previous model (a), new scale similarity model (b), and DNS data (c).

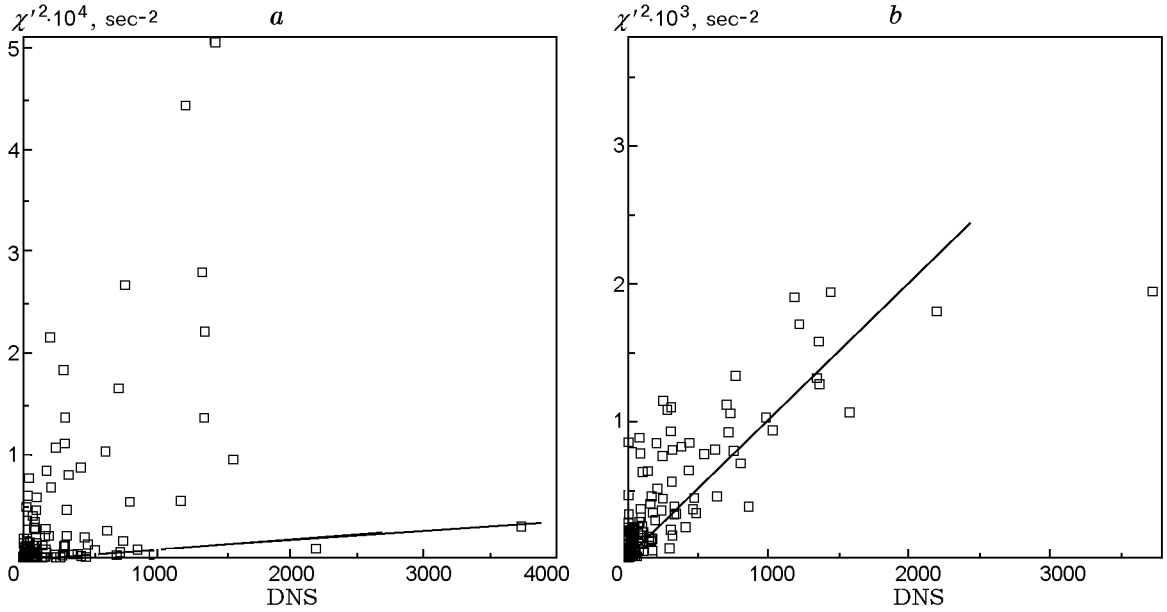

Fig. 15. Scatter plots of the actual values of $\overline{\chi'^2}$ versus the values obtained by the previous model (a) and the new model (b).

CONCLUSIONS

The direct numerical simulation of turbulent non-premixed flames of a wood pyrolysis gas, coupled with a realistic chemistry, was performed. The physical problem consists of the interaction between an initially unstrained laminar diffusion flame and a homogeneous field of decaying turbulence. The effects of turbulence on the flame structure were captured as the flame was stretched and distorted. The database obtained provides a better understanding of the turbulence flame structure and interaction between turbulence and chemistry, which is useful in improving and validating models of turbulent non-premixed combustion.

The normal displacement speed w_n is positive in the oxidizer region ($Z < 0.5$) and negative in the fuel region ($Z > 0.5$). However, negative values of w_n are observed near the $Z_{\rm st}$ region, suggesting that the fuel is locally deficient, leading the flame propagation relative to the flow field toward the fuel side. In the region near $Z_{\rm st}$, the straining motion induced by the turbulence causes the iso-Z-surfaces to move close to each other. The normal component of the displacement speed w is nearly constant, while the curvature-related component behaves in such a way to bring the curved flame to the flat flame.

Individual terms in the FSD transport equation were analyzed. The strain rate term is mainly a source as the flame surface is strained and extended. The normal displacement term w_n, which has a larger order of magnitude, contributes negatively (positively) to generation of the flame surface in the oxidizer (fuel) region. The displacement/curvature term is primarily a sink since it is dominated by the curvature component, $-\Sigma\mathcal{D}(\nabla\cdot\boldsymbol{n})^2$. This curvature term has the relatively smallest order of magnitude attributed to relatively small values of curvature.

Correlations of reaction rates with the strain rate and flame curvature are found. Reaction rates that are found to be high in regions of a high scalar dissipation rate increase with increasing positive strain rates. This is due to an increase in the flame surface area by straining. As magnitudes of curvature decrease, the reaction rates increase and reach a maximum value near zero curvature. From the correlation of strain with curvature, it is found as expected that strain rates become more positive with decreasing magnitudes of curvature as the flame is stretched. Lastly, the validity of the new model using the scale similarity assumption in obtaining closure for the mean variance of the scalar dissipation rate was examined and evaluated. The results show that the scale similarity model provides a much more accurate prediction over the existing model.

The authors wish to thank Dr. Xiangyang Zhou for many valuable discussions. We wish to acknowledge the computer support of a Beowulf cluster by the UCR-Institute of Geophysics and Planetary Physics (IGGP) for providing a parallel computing facility. The work was partially supported by the National Science Foundation under Grant No. 0049007, which is gratefully acknowledged.

REFERENCES

1. T. Poinsot, S. Candel, and A. Trouve, "Applications of direct numerical simulation to premixed turbulent combustion," *Prog. Energy Combust. Sci.*, **21**, 531–576 (1996).
2. L. Vervisch and T. Poinsot, "Direct numerical simulation of non-premixed turbulent flame," *Annu. Rev. Fluid Mech.*, **30**, 655–691 (1998).
3. D. Veynante and L. Vervisch, "Turbulent combustion modeling," *Prog. Energy Combust. Sci.,* **28**, 193–266 (2002).
4. S. Mahalingam, J. H. Chen, and L. Vervisch, "Finite-rate chemistry and transient effects in direct numerical simulations of turbulent nonpremixed flames," *Combust. Flame*, **102**, 285–297 (1995).
5. W. K. Bushe, R. W. Bilger, and G. R. Ruetsch, "Direct numerical simulation of non-premixed combustion with realistic chemistry," Tech. Report CTR Manuscript 173, Center for Turbulent Research, Standford University, Standford (1999).
6. S. Sreedhara and K. N. Lakshmisha, "Direct numerical simulation of autoignition in a nonpremixed, turbulent medium," *Proc. Symp.* (*Int.*) *Combust.*, Vol. 28, Combustion Institute, Pittsburgh (2000), pp. 25–33.
7. T. Echekki and J. H. Chen, "High-temperature combustion in autoigniting non-homogeneous hydrogen/air mixture," in: *Proc. Symp.* (*Int.*) *Combustion*, Vol. 29, Combustion Inst., Pittsburgh (2002), pp. 2061–2068.
8. N. Peters, "Laminar flamelet concepts in turbulent combustion," in: *Proc. Symp.* (*Int.*) *Combustion*, Vol. 21, Combustion Inst., Pittsburgh (1986), pp. 1231–1250.
9. F. Marble and J. Broadwell, "The coherent flame model for turbulent chemical reactions," Tech. Report No. TRW-9-PU, Project Squid Head quarters, Chaffee Hall, Purdue University (1977).
10. S. M. Candel and T. J. Poinsot, "Flame stretch and balance equation for the flame area," *Combust. Sci. Technol.*, **70**, 1–15 (1990).
11. E. Van Kalmthout, D. Veynante, and S. Candel, "Direct numerical simulation analysis of flame surface density equation in non-premixed turbulent combustion," in: *Proc. Symp.* (*Int.*) *Combustion*, Vol. 26, Combustion Inst., Pittsburgh (1996), pp. 35–42.
12. S. B. Pope, "Computational of turbulent combustion: Progress and challenges," in: *Proc. Symp.* (*Int.*) *Combustion*, Vol. 23, Combustion Inst., Pittsburgh (1990), pp. 591–612.
13. L. Vervisch, E. Bidaux, K. N. C. Bray, and W. Kollmann, "Surface density function in premixed turbulent combustion modeling similarities between probability density function and flame surface approaches," *Phys. Fluids*, **7**, 2496–2503 (1995).
14. E. van Kalmthout and D. Veynante, "Direct numerical simulation analysis of flame surface density models for nonpremixed turbulent combustion," *Phys. Fluids*, **10**, 2347–2368 (1998).
15. T. L. Clark, M. A. Jenkins, and J. Coen, and D. Packham, "A coupled atmosphere-fire model: Role of the convective Froude number and dynamic fingering at the fireline," *Int. J. Wildland Fire*, **6**, 177–190 (1996).
16. T. Echeckki and J. H. Chen, "Unsteady strain rate and curvature effects in turbulent premixed methane–air flames," *Combust. Flame*, **106**, 184–202 (1996).
17. H. G. Im and J. H. Chen, "Preferential diffusion effects on the burning rate of interacting turbulent premixed hydrogen–air flames," *Combust. Flame*, **131**, 246–258 (2002).
18. M. Z. Haq, C. G. W. Sheppard, R. Woolley, et al., "Wrinkling and curvature of laminar and turbulent premixed flame," *ibid.*, pp. 1–15.
19. C. K. Law, "Dynamics of stretched flames," in: *Proc. Symp.* (*Int.*) *Combustion*, Vol. 22, Combustion Inst., Pittsburgh (1988), pp. 1381–1402.
20. J. K. Agee, "The influence of forest structure on fire behavior," in: *Proc. Forest Vegetation Management Conf.*, Vol. 17, Redding (1996), pp. 52–68.
21. X. Zhou and S. Mahalingam, "Evaluation of reduced mechanism for modeling combustion of pyrolysis fuel gas," *Phys. Fluids*, **171**, 39–70 (2001).
22. P. K. Yeung, S. S. Grimaji, and S. B. Pope, "Straining and scalar dissipation on material surfaces in turbulence: Implication for flamelets," *Combust. Flame*, **79**, 340–354 (1990).
23. P. Domingo and L. Vervisch, "Triple flames and partially premixed combustion in autoignition of non-premixed turbulent mixtures," in: *Proc. Symp.* (*Int.*) *Combustion*, Vol. 26, Combustion Inst., Pittsburgh (1996), pp. 233–240.
24. C. J. Rutland and A. Trouvé, "Direct simulations of premixed turbulent with nonunity Lewis numbers," *Combust. Flame*, **94**, 41–57 (1993).
25. X. Zhou, W. Pakdee, and S. Mahalingam, "Assessment of flame surface density-based subgrid turbulent combustion model for nonpremixed flames of wood pyrolysis gas," *Phys. Fluids*, **16**, 3795–3807 (2004).
26. W. Pakdee and S. Mahalingam, "Accurate method to implement boundary conditions for reacting flows based on characteristic wave analysis," *Combust. Theory Modell.*, **7**, 705–729 (2003).
27. R. J. Kee, F. M. Rupley, and J. A. Miller, "CHEMKIN-II: A Fortran chemical kinetics package for the analysis of gas-phase chemical kinetics," Tech. Report No. SAND89-89009B, Sandia National Laboratories, Livermore (1989).
28. T. Passot and A. Pouquet, "Numerical simulation of compressible homogeneous flows in the turbulent regime," *J. Fluid Mech.*, **181**, 441–446 (1987).

29. L. Guichard and L. Vervisch, "Study of shock vortex interaction within a mixing zone," LMFN-CORIA No. 1993-25 (1993).
30. M. D. Smooke and V. Giovangigli, "Reduced kinetic mechanisms for asymptotic approximations for methane–air flames," *Lecture Notes Phys.*, **384**, 1–37 (1991).
31. S. K. Lele, "Compact finite difference schemes with spectral-like resolution," *J. Comput. Phys.*, **103**, 16–42 (1992).
32. F. Jacobitz, "A direct numerical study of turbulent dispersion in stratified shear flows," in: *Abstracts of the 56th Annual Meeting of the Division of Fluid Dynamics* (East Rutherford, November 23–25, 2003); *Bull. Amer. Phys. Soc.*, **48** (2003).
33. W. Gropp, E. Lusk, and A. Skjellum, *Using MPI: Portable Parallel Programming with the Message Passing Interface*, MIT Press (1999).
34. W. Klose, S. Damm, and W. Wiest, "Pyrolysis and activation of different woods — Thermo analysis (TG/EGA) and formal kinetics," in: *4th Int. Symp. of Catalytic and Thermochemical Conversions of Natural Organic Polymers*, Krasnoyarsk (2000).
35. A. Trouvé and T. Poinsot, "The evolution equation for the flame surface density in turbulent premixed combustion," *J. Fluid Mech.*, **278**, 1–31 (1994).
36. A. W. Cook, J. J. Riley, and G. Kosály, "A laminar flamelet approach to subgrid-scale chemistry in turbulent flows," *Combust. Flame*, **109**, 332–341 (1997).
37. A. W. Cook and J. J. Riley, "Subgrid-scale modeling for turbulent reacting flows," *Combust. Flame*, **112**, 593–606 (1998).
38. X. Zhou and S. Mahalingam, "A flame surface density based model for large eddy simulation of turbulent nonpremixed combustion," *Phys. Fluids*, **14**, 77–80 (2001).
39. N. Swaminathan and R. W. Bilger, "Assessment of combustion submodels for turbulent nonpremixed hydrocarbon flames," *Combust. Flame*, **116**, 519–545 (1999).
40. S. Pope, "Computations of turbulent reactive flows: Progress and challenges," *Proc. Combust. Inst.*, **23**, 591–612 (1990).
41. F. Gao and E. E. O'Brien, "A large-eddy simulation scheme for turbulent reacting flows," *Phys. Fluids, A*, **5**, 1282–1295 (1993).
42. F. A. Jaberi, P. J. Colucci, S. James, et al., "Filtered mass density function for large-eddy simulation of turbulent reacting flows," *J. Fluid Mech.*, **401**, 85–99 (1999).
43. P. Givi, "Subgrid scale modeling in turbulent combustion: A review," AIAA Paper No. 2003-5081 (2003).
44. A. W. Cook and J. J. Riley, "A subgrid model for equilibrium chemistry in turbulent flow," *Phys. Fluids*, **6**, 2868–2870 (1994).
45. N. Peters, "Local quenching due to flame stretch and non-premixed turbulent combustion," *Combust. Sci. Technol.*, **30**, 1–17 (1983).
46. S. M. de Bruyn Kops, J. J. Riley, G. Kosály, and A. W. Cook, "Investigation of modeling of non-premixed turbulent combustion," *Flow, Turb., Combust.*, **60**, 105–122 (1998).
47. P. E. Desjardin and S. H. Frankel, "Two-dimensional large eddy simulation of soot formation in the near-field of a strongly radiating nonpremixed acetylene–air turbulent jet flame," *Combust. Flame*, **119**, 121–132 (1999).
48. N. Peters and R. J. Kee, "The computation of stretched laminar methane–air diffusion flames using a reduced four-step mechanisms," *Combust. Flame*, **68**, 17–29 (1987).
49. S. P. Nandula, T. M. Brown, and R. W. Pitz, "Measurements of scalar dissipation in the reaction zones of turbulent H_2–air flames," *Combust. Flame*, **99**, 775–783 (1994).
50. J. Reveillon and L. Vervisch, "Response of the dynamic LES model to heat release induced effects," *Phys. Fluids*, **8**, 2248–2259 (1996).
51. S. Chumakov and C. J. Rutland, "Dynamic structure models for scalar flux and dissipation in large eddy simulation," *AIAA J.*, **42**, 1132–1139 (2004).
52. W. D. McComb, "The energy cascade in isotropic turbulence," in: *The Physics of Fluid Turbulence*, Vol. 25, Oxford Univ. Press, Oxford (1994), pp. 64–73.
53. D. C. Haworth and T. J. Poinsot, "Numerical simulations of Lewis number effects in turbulent flames," *J. Fluid Mech.*, **244**, 405–436 (1992).